# Transverse current fluctuations in the Yukawa one-component plasma

James P. Mithen*
*Department of Physics, University of Surrey, Guildford, Surrey GU2 7XH, United Kingdom*
(Received 4 September 2013; published 7 January 2014)

Using numerical simulations, we investigate the wave number and frequency dependent transverse current correlation function $C_T(k,\omega)$ of a single-component fluid with Yukawa interaction potential, also known as the Yukawa one-component plasma. The transverse current correlation function is an important quantity because it contains the microscopic details of the viscoelastic behavior of the fluid. We show that, in the region of densities and temperatures in which shear waves do not propagate, the dynamics of the system are in striking agreement with a simple model of generalized hydrodynamics. As either the density is increased or the temperature decreased, the transverse current correlation function shows additional structure that the simple models fail to capture.

DOI: 10.1103/PhysRevE.89.013101 PACS number(s): 52.27.Gr, 05.20.Jj

## I. INTRODUCTION

The Yukawa one-component plasma (YOCP) is a simple representation of a strongly coupled plasma, often used to describe dusty plasmas [1,2] and laser-produced plasmas [3–5]. The YOCP consists of $N$ identical point particles with charge $Ze$ and mass $m$ interacting via the Yukawa potential $v(r) = (Ze)^2 \exp(-r/\lambda_s)/4\pi\epsilon_0 r$, where $\lambda_s$ is the screening length. In equilibrium, the system is characterized by two dimensionless parameters: the coupling parameter $\Gamma = (Ze)^2/ak_bT$, where $a = (4\pi n/3)^{-1/3}$ is the average interparticle spacing, and the screening parameter $\kappa = a/\lambda_s$ [6].

Recently, there has been significant interest in the viscoelastic behavior of the YOCP [1,7,8]. The term "viscoelastic" expresses the fact that the YOCP can exhibit both dissipative and elastic responses to external disturbances. This behavior is characteristic of liquids, which exhibit dissipative (viscous) relaxation at long time and length scales but can respond elastically at short time and length scales.

Recent studies of the viscoelasticity of the YOCP have centered around the frequency dependent viscosity $\eta(\omega)$. This quantity, however, is a measure of viscoelastic behavior in the limit of large wave numbers $k \to 0$ only, i.e., at long length scales. Viscoelastic behavior at shorter (finite) length scales requires consideration of a wave number dependent quantity.

In this paper, the viscoelastic behavior of the YOCP is studied via the wave number $k$ and frequency $\omega$ dependent transverse current correlation function $C_T(k,\omega)$. At sufficiently small $k$ values, it has been shown that $C_T(k,\omega)$ can be described accurately by the conventional hydrodynamic description [9]. In this regime, the YOCP exhibits dissipative relaxation only. Extending the hydrodynamic description to higher $k$ values (shorter length scales) requires consideration of both dissipative and elastic effects, in other words, viscoelasticity.

Here, we investigate the viscoelasticity of the YOCP using the well-known framework of generalized hydrodynamics [10]. We compare one of the simplest models of generalized hydrodynamics to the results of state-of-the-art molecular dynamics (MD) simulations for $C_T(k,\omega)$. We show that, at sufficiently small coupling parameters $\Gamma$, the model is remarkably accurate for all $k$ values, i.e., the model describes both the conventional hydrodynamic limit at small $k$ values and the large $k$ behavior (when the system behaves as a collection of free particles), along with the entire intermediate dynamics between these two regimes. At higher $\Gamma$, our MD results for $C_T(k,\omega)$ exhibit peaks characteristic of propagating shear waves. We find that these shear waves are not well described by the simple models, suggesting that more complex relaxation processes are at work in these increasingly dense liquidlike states.

This paper is structured as follows. In Sec. II, we give details of our numerical simulations. In Sec. III, the generalized hydrodynamics framework is summarized, along with the Gaussian approximation for the memory function, which leads to a simple model for $C_T(k,\omega)$. This model is compared to the results of the MD simulations in Sec. IV. We first discuss the regime in which the Gaussian model is an excellent representation of $C_T(k,\omega)$ (Sec. IV A), followed by the regime in which the model fails (Sec. IV B): This is the region in which the YOCP exhibits shear waves. Concluding comments are given in Sec. V.

## II. SIMULATION DETAILS

In our MD simulations, we compute the transverse current correlation function $C_T(k,\omega)$ [10,11] of the YOCP for the $(\Gamma,\kappa)$ pairs given in Table I. In total, these pairs span a wide range of thermodynamic conditions in the fluid phase.

In our simulations, the dynamics of $N = 5000$ particles mutually interacting through the Yukawa potential are computed using the Verlet algorithm with periodic boundary conditions in a cubic box [13]. In all cases, we include the Ewald summation in our force calculation using the particle-particle–particle-mesh method [14]. The rms error of our force calculation is $10^{-5}$.

We find that obtaining accurate MD data for $C_T(k,\omega)$ requires averaging the results of a large number of simulations to improve statistics. This computational demand has made a thorough study such as this impractical before now. For example, compared with the study of Hansen for the related OCP system [15], which, even after more than 30 years remains the primary source of MD data for quantitative studies of that system [16], we use 20 times as many particles, a smaller time step by a factor of 2–10, and simulation times 200–40 000 times as large. Our time step $\delta t = 0.01\omega_p^{-1}$, where

*j.mithen@surrey.ac.uk

 

TABLE I. Screening parameters $\kappa$ and coupling parameters $\Gamma$ for which MD simulations of the transverse current correlation function $C_T(k,\omega)$ were carried out. At $\kappa = 0.1, 1$ and 2, the melting point of the system is $\Gamma_m \approx 172.2$, 217.4, and 440.1, respectively [12].

| $\kappa$ | $\Gamma$ |
|---|---|
| 0.1 | 1,5,10,50,120,175 |
| 1 | 1,5,10,50,90,120,175,200 |
| 2 | 1,5,10,50,120,175,200,300,350,400 |

$\omega_p = \sqrt{Z^2e^2n/\epsilon_0 m}$ is the plasma frequency, ensures excellent energy conservation ($\Delta E/E \approx 10^{-5}$). Moreover, we find that the long length of our simulations, $25 \times 819.2\omega_p^{-1}$ for every $\Gamma$ and $\kappa$ value, is of paramount importance: While it is possible to capture the essential features of $C_T(k,\omega)$ with simulations significantly shorter than this, producing a spectrum that is of sufficient accuracy to draw conclusions about the validity of various models requires simulations of approximately this length [we note that our data for $C_T(k,\omega)$ changes negligibly by increasing the simulation time beyond $25 \times 819.2\omega_p^{-1}$].

## III. MODELS FOR $C_T(k,\omega)$

### A. Generalized hydrodynamics description

In the hydrodynamic regime, governed by the linearized Navier-Stokes equations, the time evolution of the transverse current correlation function is given by [17]

$$\frac{\partial}{\partial t} C_T(k,t) = -\eta k^2 C_T(k,t), \tag{1}$$

where $\eta$ is the shear viscosity. The resulting exponential decay of $C_T(k,t)$ leads to a Lorentzian in frequency space,

$$C_T(k,\omega) = \frac{k_B T}{m\pi} \frac{\eta k^2}{\omega^2 + (\eta k^2)^2}, \tag{2}$$

where the exact result $C_T(k,t=0) = k_B T/m$ has been used. The simple description given by Eqs. (1) and (2) can only be expected to be accurate in the hydrodynamic regime. It was recently shown that this regime can be characterized for the YOCP by the maximum wave number $k_{\max}$ at which the Navier-Stokes description applies, given by $k_{\max}\lambda_s \simeq 0.43$ [4,9]. Beyond $k = k_{\max}$, Eq. (1) is no longer satisfied and approaches beyond conventional hydrodynamics are needed.

A natural way to proceed is via the framework of generalized hydrodynamics [10,11,17]. In this approach, the time evolution of $C_T(k,t)$ is written as

$$\frac{\partial}{\partial t} C_T(k,t) = -k^2 \int_0^t dt' \phi(k,t-t') C_T(k,t'), \tag{3}$$

where $\phi_T(k,t)$ is known as the memory function [10,17,18]. Equation (3) leads to the generalized hydrodynamics description

$$C_T(k,\omega) = \frac{k_B T}{m\pi} \frac{k^2\phi'(k,\omega)}{[\omega - k^2\phi''(k,\omega)]^2 + [k^2\phi'(k,\omega)]^2}, \tag{4}$$

where $\phi'(k,\omega)$ and $\phi''(k,\omega)$ are, respectively, the real and imaginary parts of the Laplace transform of the memory function $\phi(k,t)$.

Equation (4) is a well-known and exact representation of $C_T(k,\omega)$; it can be formally derived from microscopic theory [10]. The advantage of this particular representation is its similarity to the conventional hydrodynamic description: As can be seen by comparing Eqs. (2) and (4), the memory function plays the role of a generalized viscosity. This makes the memory function a natural formalism with which to investigate the viscoelastic behavior of the YOCP.

### B. Model for $C_T(k,\omega)$

In order to specify a model for $C_T(k,\omega)$, an approximation to the memory function is needed. The model we present here amounts to using the Gaussian ansatz for the memory function,

$$\begin{aligned} k^2\phi(k,t) &= k^2\phi(k,0)\exp\left(-\pi t^2/4\tau_k^2\right) \\ &= \omega_T^2(k)\exp\left(-\pi t^2/4\tau_k^2\right), \end{aligned} \tag{5}$$

where $\omega_T^2(k)$ is given by the second frequency moment of $C_T(k,\omega)$ [10]. An exact expression for $\omega_T^2(k)$ in terms of the radial distribution function $g(r)$ is given in the Appendix. The parameter $\tau_k$ in Eq. (5) is a wave number dependent relaxation time. According to Eq. (5), the real and imaginary parts of the Laplace transform of the memory function are given by, respectively [15,18],

$$k^2\phi'(k,\omega) = \omega_T^2(k)\tau_k e^{-\tau_k^2\omega^2/\pi} \tag{6}$$

and

$$k^2\phi''(k,\omega) = \frac{2\tau_k}{\sqrt{\pi}}\omega_T^2(k) D(\tau_k\omega/\sqrt{\pi}), \tag{7}$$

where the Dawson function $D(x) = \exp(-x^2)\int_0^x \exp(y^2)dy$ [19].

Where appropriate, we also compare the MD results with a second model, which amounts to using the exponential ansatz for the memory function,

$$\begin{aligned} k^2\phi(k,t) &= k^2\phi(k,0)\exp(-t/\tau_k) \\ &= \omega_T^2(k)\exp(-t/\tau_k), \end{aligned} \tag{8}$$

In this case, the real and imaginary parts of the Laplace transform that appear in Eq. (4) are given by

$$k^2\phi'(k,\omega) = \frac{\omega_T^2(k)\tau_k}{1+\omega^2\tau_k^2} \tag{9}$$

and

$$k^2\phi''(k,\omega) = \frac{\omega_T^2(k)\omega\tau_k}{1+\omega^2\tau_k^2}. \tag{10}$$

Confusingly, this second model is sometimes called the viscoelastic model in the literature; however, in reality the exponential memory function model in Eqs. (8)–(10) is one of many possible ways to describe viscoelastic behavior phenomenologically (and the Gaussian model is another).

### C. Physical motivation for the memory function models

From its definition in Eq. (3), it is clear why $\phi(k,t)$ is called the memory function: The decay rate of $C_T(k,t)$ depends on its past history and $\phi(k,t)$ controls to what extent $C_T(k,t)$ "remembers its past history" [17]. Comparing Eqs. (1) and (3),

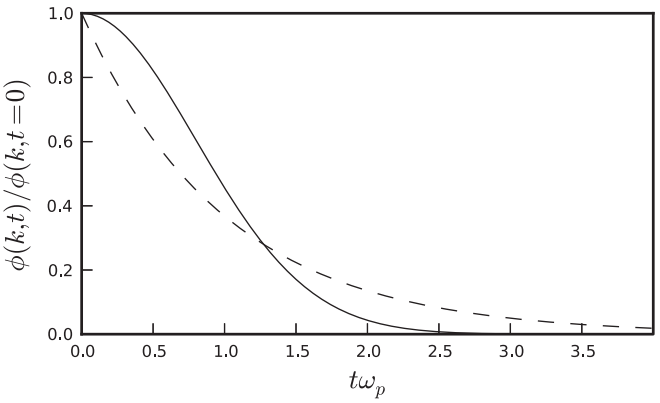


FIG. 1. Memory function in the time domain for Gaussian (solid line) and exponential (dashed line) models, for $\tau_k\omega_p = 1$.

we can see that the memory function corresponding to ordinary hydrodynamics is

$$\phi(k,t) = 2\eta\delta(t). \tag{11}$$

In other words, ordinary Navier-Stokes hydrodynamics makes the assumption that the system is memoryless.

By taking the memory function to be time dependent, we introduce a time scale $\tau_k$. Physically, $\tau_k$ can be thought of as the time the system takes to adjust itself to an external probe [10]. We expect that if we probe the system at time scales that are long compared to $\tau_k$, that is, at low frequencies $\omega$ satisfying $\omega\tau_k \ll 1$, the system has sufficient time to adjust to the probe. In the opposite regime $\omega\tau_k \gg 1$, the system is frozen; it cannot follow the rapid variation of the external probe. Thus, in the former limit the system responds as a viscous fluid, whereas in the latter limit it behaves like an elastic solid.

Both of the memory function models presented in the previous section are essentially phenomenological ways of interpolating between these two limiting cases. We can discuss the physical intuition in the difference between the two models with reference to Fig. 1, which shows the memory function in the time domain, normalized by its initial value, for both models. In Fig. 1, we have taken $\tau_k\omega_p = 1$, but this qualitative discussion is valid for any value of $\tau_k$ [20]. Coming from the right-hand side of Fig. 1, that is, at long times, the exponential memory function is non-negligible, whereas the Gaussian memory function is essentially zero. Physically then, appreciable elastic behavior sets in at shorter time scales (higher frequency) for the exponential model than for the Gaussian model. At time $t_M = 4\tau_k/\pi$, the two memory functions are equal. At times shorter than $t_M$, the Gaussian memory function is larger than the exponential memory function. Overall then, the Gaussian model exhibits stronger elastic behavior than the exponential model at short times $t < t_M$, but as time increases this elasticity dies away more rapidly than for the exponential model. For further discussion of these two models, the reader is referred to Ref. [10] and references therein.

### D. Connection to prior work

The Gaussian model has previously been applied extensively to modeling the longitudinal current correlation function (i.e., the dynamical structure factor [11]) of the Lennard-Jones fluid [18,21] and the OCP [15]; in this context it has also been applied to experimental data for weakly coupled plasma produced by arc jets [22]. Furthermore, for the YOCP, it was recently shown that the Gaussian model is an extremely accurate representation of the dynamical structure factor for a wide range of thermodynamic conditions [23].

In this paper, we are interested in the transverse current correlation function. The Gaussian model has also been applied in this context for other systems [18,21]. However, because of the difficulty of conducting highly accurate numerical simulations at the time of these previous investigations, a detailed, conclusive comparison of the model with the results of MD simulations was not possible for those systems.

Here, with the aid of modern computers, we have conducted accurate large-scale MD simulations for $C_T(k,\omega)$ across a wide range of thermodynamic conditions. We find that, at sufficiently small coupling parameters $\Gamma$, the Gaussian model provides an extremely accurate description of $C_T(k,\omega)$ for all $k$ values, i.e., the model describes both the conventional hydrodynamic limit at small $k$ values and the large $k$ behavior (when the system behaves as a collection of free particles), along with the entire intermediate dynamics between these two regimes.

At higher $\Gamma$, our MD results for $C_T(k,\omega)$ exhibit peaks characteristic of propagating shear waves. We find that these shear waves cannot be well described by the Gaussian model or indeed other approximations to the memory function that involve a single relaxation time (such as the exponential model). This suggests that the more complex relaxation processes in these increasingly dense liquidlike states are more readily accessed by studying the transverse current correlations rather than the longitudinal current correlations, for which the Gaussian model was recently shown to be accurate [4]. Experiments designed to probe the transverse current fluctuations [1] could therefore be a rich source of information on the collective dynamics of dense plasmas.

## IV. RESULTS AND ANALYSIS

In order to compare the Gaussian memory function model given in Eqs. (4), (6), and (7) with the MD results, values for the two parameters $\omega_T^2(k)$ and $\tau_k$ are needed for each $k$. Since these two parameters are in general unknown, we have fitted them to the MD spectrum of $C_T(k,\omega)$ using the least-squares method. That is to say, for each $k$ value for which we have computed $C_T(k,\omega)$ with MD (these are the $k$ values compatible with the periodic boundary conditions in our simulations), we fit the model to the MD spectrum of $C_T(k,\omega)$.

This two-parameter fit is the best way to compare the Gaussian memory function model to the MD spectrum of $C_T(k,\omega)$. This is true despite the fact that the parameter $\omega_T^2(k)$ can in principle be obtained by computing the radial distribution function $g(r)$ (or equivalently the static structure factor $S(k)$ [11]) with MD and using the formula for $\omega_T^2(k)$ given in the Appendix. When obtained from MD in this way, $\omega_T^2(k)$ is subject to numerical uncertainty. Therefore, one would expect that constraining this parameter, and therefore fitting the model to the MD spectrum using only a single parameter $\tau_k$ [15,18,22], would result in poorer fits and larger

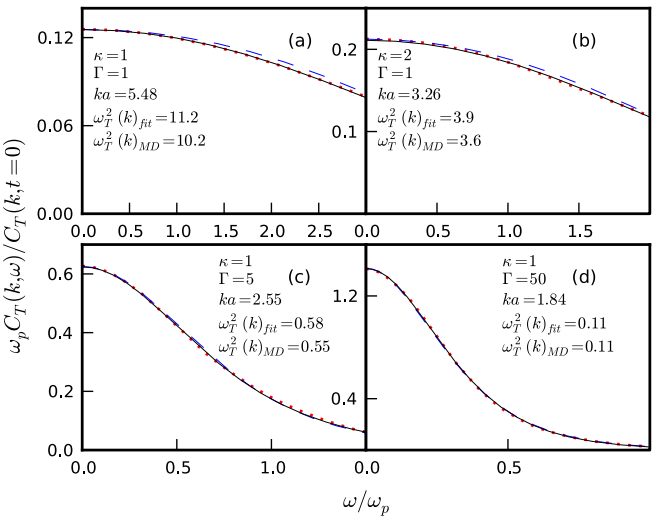


FIG. 2. (Color online) Comparison between the Gaussian model when only the parameter $\tau_k$ is fitted to the MD spectrum (dashed line) and when both $\tau_k$ and $\omega_T^2(k)$ are fitted (solid line) for four separate cases. The MD results are given by the dots.

errors. In Fig. 2, we show that in general this is indeed the case.

The validity of the two parameter fit can be confirmed by comparing the fitted value of $\omega_T^2(k)$ to its value when instead computed with MD as described above. As shown in Fig. 3, the value of $\omega_T^2(k)$ obtained from the fit to the MD spectrum of $C_T(k,\omega)$ agrees very well (within 10%) with that computed from the MD $g(r)$. This is only the case because the model gives an accurate representation of $C_T(k,\omega)$. For example, as shown in Fig. 3, if an exponential rather than Gaussian memory function is used, the numerical value obtained for $\omega_T^2(k)$ by fitting the model with two parameters does not agree well with the value computed from the MD $g(r)$.

In the remainder of this section, we present only the results for the Gaussian memory function model with two fitting parameters; the one parameter fits are irrelevant as their comparison with the MD data for $C_T(k,\omega)$ is not indicative of the quality of the model.

### A. Comparison between the model and MD simulations

The main result of this paper is that, in the region of $(\Gamma,\kappa,k)$ space in which shear waves do not propagate, the Gaussian memory function model reproduces the MD spectrum of $C_T(k,\omega)$ very accurately. We first present our results in this region, before discussing the more problematic (but physically more interesting) shear wave region in Sec. IV B. Because of the large volume of data generated by our simulations, extended figures of our complete MD results are available in Supplemental Material [24]; here, we show only a selection of these complete results. Our simulations cover the range $ka = 0.23$–$6.19$.

In Fig. 4, we compare the model to the MD spectrum of $C_T(k,\omega)$ for the smallest $k$ value accessible to our simulation, $ka = 0.23$. Clearly, the model provides an accurate description of the MD results. This is to be expected since for this small value of $k$ we are within the hydrodynamic regime [4,9]. In

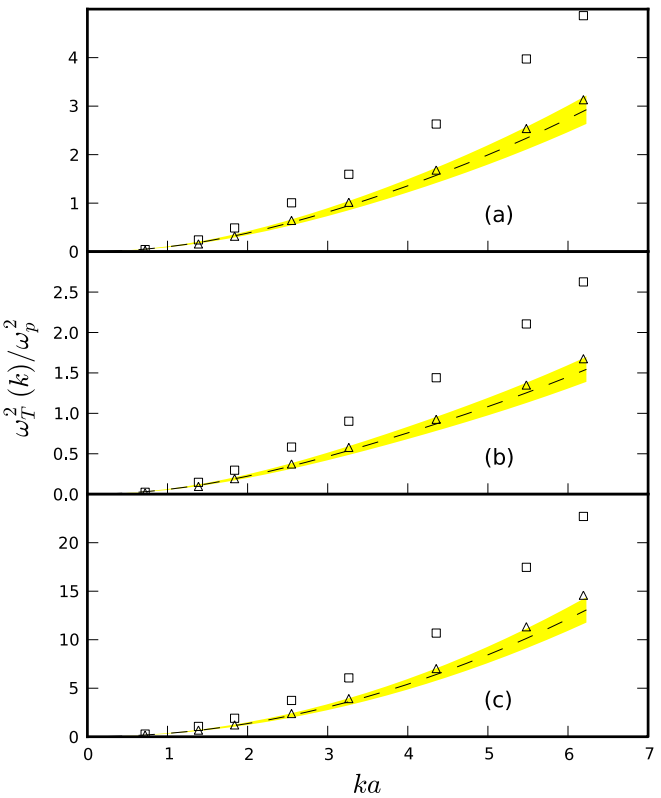


FIG. 3. (Color online) Comparison between $\omega_T^2(k)$ as computed from MD using the formula in the Appendix (dashed line, with 10% error band) and the values obtained from the two-parameter fit of the Gaussian memory function model (triangles) and the exponential model (squares) for three different $(\Gamma,\kappa)$ pairs: (a) $\Gamma = 5$, $\kappa = 0.1$; (b) $\Gamma = 10$, $\kappa = 1$; and (c) $\Gamma = 1$, $\kappa = 2$.

this regime, $\phi_T'(k,\omega)$ reduces to the shear viscosity $\eta$ and $\phi_T''(k,\omega)$ vanishes. This means that the generalized hydrodynamics description of Eq. (4) reduces to the conventional hydrodynamic description of Eq. (2) [10]. At larger $k$ values,

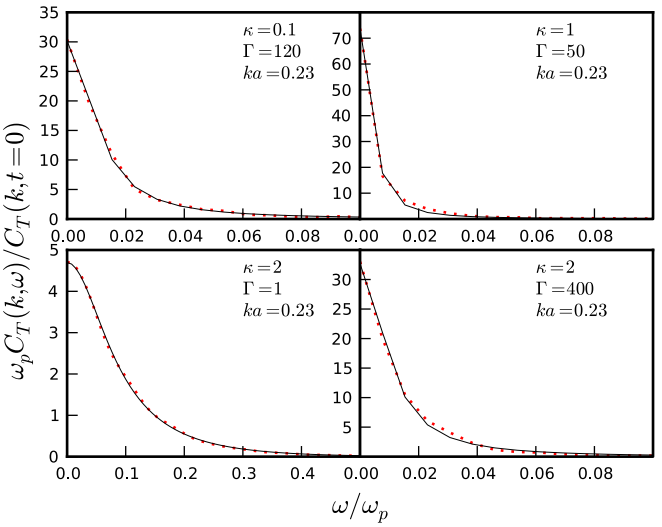


FIG. 4. (Color online) Comparison between the MD data for $C_T(k,\omega)$ (dots) and the Gaussian memory function model with two fitting parameters (solid line) for the smallest $ka$ value accessible to our simulations.

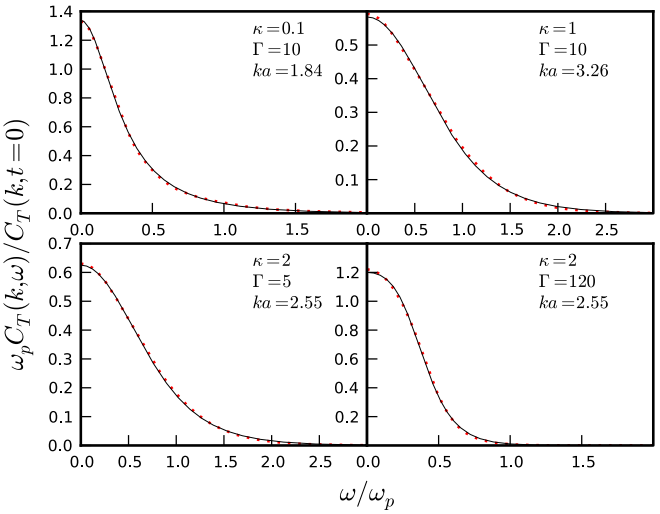


FIG. 5. (Color online) Comparison between the MD data for $C_T(k,\omega)$ (dots) and the Gaussian memory function model with two fitting parameters (solid line) for intermediate $ka$ values.

as shown in Figs. 5 and 6, the model extends the conventional hydrodynamic description; here, the real part of $\phi(k,\omega)$ corrects for the peak width.

Clearly, in the region of $(\Gamma,\kappa,k)$ space that accommodates the conditions in Figs. 4–6, the MD spectrum of $C_T(k,\omega)$ consists of a single peak at $\omega = 0$. In this region, there are no propagating shear waves observed in the MD data, which would be seen as a peak at nonzero frequency. The single $\omega = 0$ peak in $C_T(k,\omega)$ corresponds to a monotonic decay of transverse current fluctuations in the time domain. In this region, the Gaussian model provides an excellent description of $C_T(k,\omega)$.

### B. Onset of shear waves

As $\Gamma$ increases for a given screening parameter $\kappa$, the YOCP becomes increasingly liquidlike. In common with ordinary liquids, the system can then support waves that propagate perpendicular to the particle velocities, that is, shear waves [11].

In the time domain, the onset of shear waves occurs at the smallest wave number for which the transverse current correlation function becomes negative [25,26]. This wave number is sometimes referred to as the cutoff wave number [7]. In this sense transverse (shear) waves are different from longitudinal (sound) waves since the latter are supported by the system all the way to $k = 0$.

The onset of shear waves is evidenced by a peak in $C_T(k,\omega)$ at nonzero frequency $\omega(k)$. We find such a peak in our MD results for $\kappa = 0.1$ when $\Gamma \geqslant 50$, for $\kappa = 1$ when $\Gamma \geqslant 50$, and for $\kappa = 2$ when $\Gamma \geqslant 120$. As a fraction of the melting point of the system, this corresponds to $\Gamma/\Gamma_m \geqslant 0.29$, 0.23, and 0.27 respectively [12]. However, given the limited number of $\Gamma$ values for which we have performed MD simulations (see Table I), it is likely that shear waves can propagate at a slightly lower fraction of the melting point.

In Fig. 7, we show how $\omega(k)$, the frequency of the shear wave, changes as $\Gamma$ and $\kappa$ are varied. As shown in Fig. 7, for small $k$, $\omega(k)$ increases as $k$ increases, which is consistent with previous calculations [26]. Beyond $ka = 3$, $\omega(k)$ decreases to a minimum before increasing again. We note that this second part of the dispersion curve is only present in the very strongly coupled regime, when $\Gamma$ is greater than $\approx 0.5\Gamma_m$. In this region, $C_T(k,\omega)$ exhibits considerable structure (see Fig. 9 and further images in Ref. [24]). Indeed, at these relatively short length scales, both single-particle and collective effects are important.

Figure 7(a) shows that the dispersion curves are similar for $\kappa = 0.1$ and 1 at fixed $\Gamma$; this is presumably because the melting point $\Gamma_m$ is similar for these two values of $\kappa$ [7].

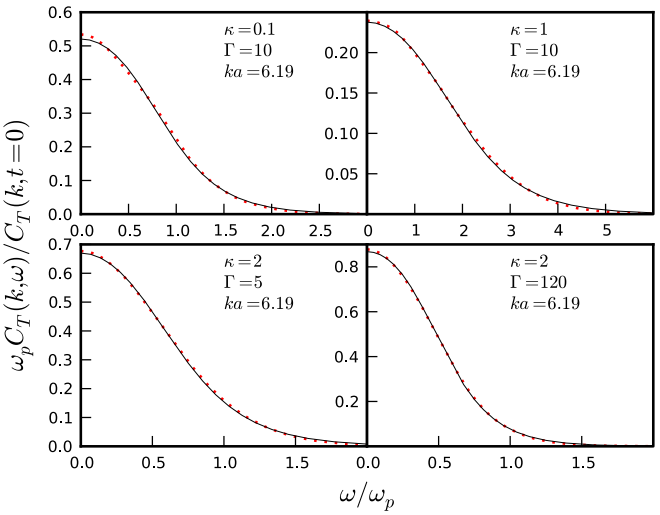


FIG. 6. (Color online) Comparison between the MD data for $C_T(k,\omega)$ (dots) and the Gaussian memory function model with two fitting parameters (solid line) for large $ka$ values.

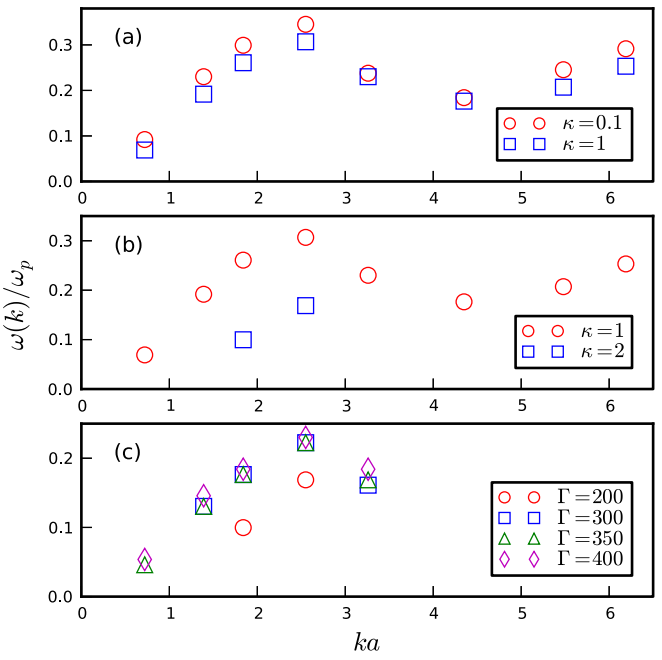


FIG. 7. (Color online) Position of shear wave peak $\omega(k)$ for (a) $\kappa = 0.1$ and 1 at a fixed coupling parameter $\Gamma = 175$, (b) $\kappa = 1$ and 2 at a fixed coupling parameter $\Gamma = 200$, and (c) $\Gamma = 200$, 300,350,400 at fixed screening parameter $\kappa = 2$.

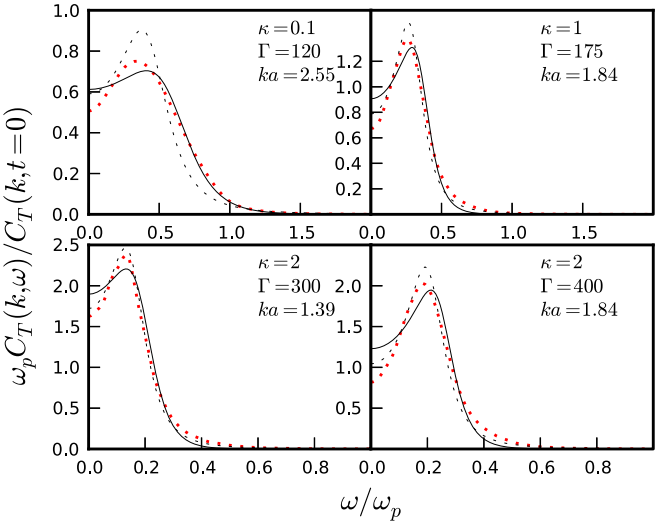


FIG. 8. (Color online) Comparison between the MD data for $C_T(k,\omega)$ (dots) and the Gaussian memory function model with two fitting parameters (solid line) in the region of shear wave propagation. Also shown is the exponential memory function model (dashed line).

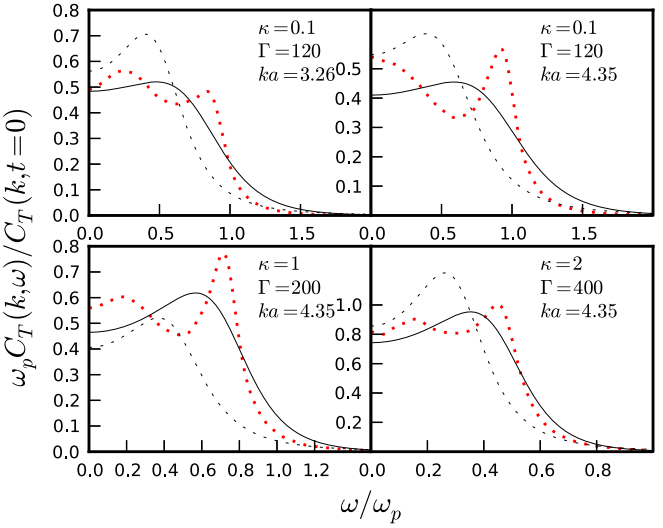


FIG. 9. (Color online) Comparison between the MD data for $C_T(k,\omega)$ (dots) and the Gaussian memory function model with two fitting parameters (solid line). Also shown is the exponential memory function model (dashed line).

Consistent with this reasoning, Fig. 7(b) shows a greater difference between the dispersion curves for $\kappa = 1$ and 2 than for $\kappa = 0.1$ and 1. We also note that the cutoff wave number below which shear waves do not propagate is found to be larger as $\kappa$ increases, in agreement with previous calculations [7]. No propagating shear wave is detected in the MD data for $\kappa = 2$ beyond $ka \approx 3$. At fixed $\kappa$, $\omega(k)$ increases with $\Gamma$, as shown in Fig. 7(c). This is particularly obvious when going from $\Gamma = 200$ to 300, which correspond to $\Gamma/\Gamma_m \approx 0.45$ and 0.68, respectively. Intuitively, as $\Gamma/\Gamma_m$ increases, the restoring force for collective fluctuations increases and hence $\omega(k)$ increases. For $\Gamma \geqslant 300$, $\omega(k)$, and indeed the entire function $C_T(k,\omega)$, remains remarkably similar.

In Figs. 8 and 9, we compare the memory function models to the MD data in the region of $(\Gamma,\kappa,k)$ space in which shear waves propagate. In Fig. 8, we show results for $k \leqslant 3$, when $C_T(k,\omega)$ consists of a single peak at nonzero frequency. Here, the Gaussian model can indeed capture the overall shape of $C_T(k,\omega)$. However, in general the model tends to slightly overestimate the peak frequency, which can be thought of as the strength of elasticity effects, and also overestimate the contribution to $C_T(k,\omega)$ at zero frequency, i.e., the dissipative effects. In Fig. 8, we also plot the results of the exponential memory function model, which is also frequently used in the literature [10,11,17,18,21,27]. It can be seen that the exponential memory function model is more sharply peaked than the MD data, but it exhibits a smaller value of $C_T(k,\omega = 0)$, which is closer to the MD data. We note that the relative peak frequencies and peak widths resulting from the two models can be rationalized in terms of the qualitative discussion given in Sec. III C.

At higher $k$ values, as shown in Fig. 9, $C_T(k,\omega)$ is found to exhibit a two-peak structure. Given the relatively high frequency of the second peak, it is likely this is due to caging effects (e.g., [4,10,11]). In other words, at these length scales the relatively-high-frequency oscillations of individual particles in the cages produced by their neighbors are imprinted on $C_T(k,\omega)$. We note that this second peak occurs at approximately the frequency at which the longitudinal dispersion relation plateaus [6,23]. This observation lends support to the idea that the peak is due to caging: One would expect these single particle (noncollective) dynamics to occur at the same frequency in both transverse and longitudinal current fluctuations. In any case, both the Gaussian and exponential models fail to describe the two peak structure, which is to be expected, as approximations to the memory function that involve a single relaxation time can only ever describe a single resonance.

## V. CONCLUDING COMMENTS

The Gaussian memory function model is an extremely accurate representation of the transverse current correlation function $C_T(k,\omega)$ of the YOCP in the region of $(\Gamma,\kappa,k)$ space in which shear waves do not propagate. This region is $\Gamma \lesssim 0.25\Gamma_m$, where $\Gamma_m$ is the melting point, which depends on $\kappa$. At a given value of $\kappa$, providing $\Gamma$ is in this region, the model works well for all $k$ values (i.e., at all length scales). This conclusion was possible only because of the highly accurate MD data presented in this paper. Figures of the complete MD data for $C_T(k,\omega)$ are available in Ref. [24].

Why exactly the Gaussian model is superior to the exponential model in this region is an interesting question. Here, the accuracy of the Gaussian model is presented as an empirical observation, but attempting to motivate this from first principles would certainly be worthwhile, albeit challenging [10].

The model can be used by fitting either a single parameter or two parameters to the spectrum of $C_T(k,\omega)$ at a particular $k$ value. The advantage of using two parameters is that the small numerical inaccuracies that arise in the MD simulations can be accounted for.

In the shear wave region, $C_T(k,\omega)$ shows a distinct peak at a nonzero frequency, which is poorly characterized by the

Gaussian model. When even more structure in $C_T(k,\omega)$ is present, the model breaks down completely.

Recently, the same memory function model used here was shown to accurately describe the longitudinal current correlations of the YOCP, even in the region in which it has been found to break down for the transverse current correlations [4]. This suggests the complex relaxation behavior of dense liquidlike plasmas can in some cases be more readily accessed by studying the transverse rather than longitudinal current correlations. Experiments designed to probe the transverse current fluctuations [1] could therefore be a rich source of information on the collective dynamics of dense plasmas.

## ACKNOWLEDGMENTS

This work was partly supported by the John Fell Fund at the University of Oxford and by EPSRC Grant No. EP/G007187/1. The author would like to thank Jerome Daligault at LANL for many inspiring discussions.

## APPENDIX: EXACT EXPRESSION FOR $\omega_T^2(k)$

The wave number dependent quantity $\omega_T^2(k)$ can be written in terms of the frequency moments of $C_T(k,\omega)$,

$$\langle\omega^n\rangle = \int_{-\infty}^{\infty} \omega^n C_T(k,\omega)d\omega. \tag{A1}$$

In terms of these frequency moments, we have [10]

$$\omega_T^2(k) = \frac{\langle\omega^2\rangle}{\langle\omega^0\rangle}. \tag{A2}$$

The zeroth frequency moment can easily be calculated as

$$\langle\omega^0\rangle = \frac{k_B T}{m}. \tag{A3}$$

Using this result, $\omega_T^2$ can be written as [see [10], Eq. (1.151)]

$$\omega_T^2(k) = \frac{k_B T}{m}k^2 + \Omega_E^2 - \Omega_k^2. \tag{A4}$$

Here, $\Omega_E$ is the Einstein frequency, which for the YOCP is

$$\Omega_E^2 = \frac{\kappa^2}{3}\int_0^{\infty} \bar{r}\exp(-\kappa\bar{r})g(\bar{r})d\bar{r}, \tag{A5}$$

where $\bar{r} = r/a$ and $g(r)$ is the radial distribution function [11]. For the YOCP, the remaining term is

$$\Omega_k^2 = \frac{1}{3}\int_0^{\infty} \bar{r}^2 g(\bar{r}a)\exp(-\kappa\bar{r})\left[\frac{\sin kr}{kr}\frac{\kappa^2}{\bar{r}} + \frac{3}{(kr)^2}\left(\frac{\sin kr}{kr} - \cos kr\right) - \frac{\sin kr}{kr}\left(\frac{3}{\bar{r}^3} + \frac{3\kappa}{\bar{r}^2} + \frac{\kappa^2}{\bar{r}}\right)\right]. \tag{A6}$$

Using Eqs. (A4)–(A6), the value of $\omega_T^2(k)$ can be computed for a particular values of $\Gamma$, $\kappa$, and $k$ provided $g(r)$ is known.


[1] P. Hartmann, M. C. Sandor, A. Kovacs, and Z. Donkó, Phys. Rev. E **84**, 016404 (2011).

[2] H. Totsuji, T. Kishimoto, C. Totsuji, and T. Sasabe, Phys. Rev. E **58**, 7831 (1998).

[3] M. S. Murillo, Phys. Rev. E **81**, 036403 (2010).

[4] J. P. Mithen, J. Daligault, and G. Gregori, Phys. Rev. E **83**, 015401(R) (2011).

[5] J. Vorberger, Z. Donkó, I. M. Tkachenko, and D. O. Gericke, Phys. Rev. Lett. **109**, 225001 (2012).

[6] Z. Donkó, G. J. Kalman, and P. Hartmann, J. Phys.: Condens. Matter **20**, 413101 (2008).

[7] J. Goree, Z. Donkó, and P. Hartmann, Phys. Rev. E **85**, 066401 (2012).

[8] Z. Donkó, P. Hartmann, and P. K. Shukla, Phys. Lett. A **376**, 3199 (2012).

[9] J. P. Mithen, J. Daligault, and G. Gregori, Contrib. Plasma Phys. **52**, 58 (2012).

[10] U. Balucani and M. Zoppi, *Dynamics of the Liquid State* (Oxford University Press, Oxford, 2002).

[11] J. P. Hansen and I. R. McDonald, *Theory of Simple Liquids*, 3rd ed. (Academic, New York, 2006).

[12] H. Ohta and S. Hamaguchi, Phys. Plasmas **7**, 4506 (2000).

[13] M. P. Allen and D. J. Tildesley, *Computer Simulation of Liquids* (Oxford University Press, Oxford, 1987).

[14] R. Hockney and J. Eastwood, *Computer Simulations Using Particles* (McGraw-Hill, New York, 1981).

[15] J. P. Hansen, I. R. McDonald, and E. L. Pollock, Phys. Rev. A **11**, 1025 (1975).

[16] Yu. V. Arkhipov, A. Askaruly, D. Ballester, A. E. Davletov, I. M. Tkachenko, and G. Zwicknagel, Phys. Rev. E **81**, 026402 (2010).

[17] J. P. Boon and S. Yip, *Molecular Hydrodynamics* (Dover, New York, 1980).

[18] N. K. Ailawadi, A. Rahman, and R. Zwanzig, Phys. Rev. A **4**, 1616 (1971).

[19] A method for implementing the Dawson function can be found in W. H. Press, S. A. Teukolsky, W. T. Vetterling, and B. P. Flannery, *Numerical Recipes in C: The Art of Scientific Computing*, 2nd ed. (Cambridge University Press, Cambridge, 1992).

[20] Here we are assuming that $\tau_k$ is the same for both models. This appears to be true to a good approximation from the MD fits we have performed.

[21] I. M. de Schepper, E. G. D. Cohen, C. Bruin, J. C. van Rijs, W. Montfrooij, and L. A. de Graaf, Phys. Rev. A **38**, 271 (1988).

[22] G. Gregori, U. Kortshagen, J. Heberlein, and E. Pfender, Phys. Rev. E **65**, 046411 (2002).

[23] J. P. Mithen, J. Daligault, B. J. B Crowley, and G. Gregori, Phys. Rev. E **84**, 046401 (2011).

[24] See Supplemental Material at http://link.aps.org/supplemental/10.1103/PhysRevE.89.013101 for these extended $C_T(k,\omega)$ figures. The numerical data for these figures can be obtained by contacting the author.

[25] U. Balucani, J. P. Brodholt, P. Jedlovszky, and R. Vallauri, Phys. Rev. E **62**, 2971 (2000).

[26] Z. Donkó, J. Goree, and P. Hartmann, Phys. Rev. E **81**, 056404 (2010).

[27] N. H. March and M. P. Tosi, *Atomic Dynamics in Liquids* (Dover, New York, 1991).